

Estimation of Flight State with a Collision Alert Radar

Maas, J.B.; van Gent, R.N.H.W.; Hoekstra, J.M.

DOI

[10.2514/1.1010898](https://doi.org/10.2514/1.1010898)

Publication date

2021

Document Version

Final published version

Published in

Journal of Aerospace Information Systems (online)

Citation (APA)

Maas, J. B., van Gent, R. N. H. W., & Hoekstra, J. M. (2021). Estimation of Flight State with a Collision Alert Radar. *Journal of Aerospace Information Systems (online)*, 18(6), 347-354.
<https://doi.org/10.2514/1.1010898>

Important note

To cite this publication, please use the final published version (if applicable).
Please check the document version above.

Copyright

Other than for strictly personal use, it is not permitted to download, forward or distribute the text or part of it, without the consent of the author(s) and/or copyright holder(s), unless the work is under an open content license such as Creative Commons.

Takedown policy

Please contact us and provide details if you believe this document breaches copyrights.
We will remove access to the work immediately and investigate your claim.



Estimation of Flight State with a Collision Alert Radar

Jerom Maas,*^{ORCID} Ronald van Gent,[†] and Jacco Hoekstra[‡]
Delft University of Technology, 2629 HS Delft, The Netherlands

<https://doi.org/10.2514/1.1010898>

It was found that a newly developed portable collision alert radar receives reflections from the ground while flying. In this paper a method is developed that uses range and Doppler information from these reflections. This information is used to compute height and velocity information relative to the terrain, something which is not possible with existing hardware. The method was tested on a local flight in the Netherlands, with a prototype of the radar. Flight state results were compared with those of a GPS tracker on board. It was found that the velocity can be computed within meters-per-second accuracy. Height differences are due to the measurement method, measuring directly from the ground surface (radar) or relative to a database (GPS). If developments in microwave sensing techniques continue to improve the hardware, flight state estimation by radar can become an option for pilots who do not want to be dependent on the correctness of a terrain model, but who measure the terrain shape independently.

Nomenclature

A	=	aircraft position
altitude	=	vertical distance of aircraft above mean sea level, computed by a barometer
elevation	=	vertical distance of ground above mean sea level
H	=	height of aircraft above ground
height	=	vertical distance between aircraft and ground
p	=	a point on the ground
r	=	distance from the aircraft to the object observed by the radar
SD	=	standard deviation
T	=	aircraft track vector
V	=	aircraft velocity vector
V_r	=	Doppler velocity of the object observed by the radar
V_x	=	horizontal velocity of the aircraft
V_z	=	vertical velocity of the aircraft

I. Introduction

AN AIRBORNE collision alert radar is being developed for use in general aviation (GA) [1,2]. Although its primary goal is not to detect the ground, reflections from the surface are observed in the radar output. These reflections can contain useful information for a GA pilot, because it is crucial to know the aircraft state with respect to the landscape.

The traditional flight instruments of an aircraft provide the pilot with the state information by interpreting the air data. A barometric altimeter can compute the distance above the runway. If the altimeter is set correctly, the altitude is 0 when the aircraft lands on the runway. This way of setting the altimeter will be used in the rest of this paper, but it does not provide information about the landscape around the airfield [3].

Inertial Navigation Systems (INS) track the aircraft position by dead reckoning from takeoff, and satellite-based navigation (GPS) is used in commercially available navigation apps [4–6]. These systems determine the sensor position with respect to the start of the flight (INS), or with respect to an elliptical approximation of the Earth mean sea level (GPS). None of these instruments measure the surface, but the position of the ground is stored in an internal model of the elevation. But this map may be outdated or lack detail, and tree

tops increase the terrain height that a pilot wants to avoid, which may not be included in the database. Such faults can lead to unsafe situations.

In order not to rely on an elevation map, it is possible to perform direct measurements on the surface. This can be done with a radar or light detection and ranging (lidar) altimeter [7,8]. These systems measure the distance to the ground directly below the aircraft. This provides information from a single point and not about the entire landscape. For collision warnings about the landscape in front of the aircraft, the pilot is still dependent on an internal elevation model. The limited functionality of lidar altimetry, combined with a steep price, is the reason that lidar altimeters are not often used in GA.

Progress in the field of microwave sensing has empowered the development of new portable radar hardware for direct measurements [9]. Such a new system can be used in GA, as a collision alert radar. Example functionalities are to detect wind turbines and to track aircraft in 3D. The equipment will cost less than a complete ADS-B/CDTI[§] combination, and all “sense and avoid” functions can be performed simultaneously by a single machine. The application of portable radar in GA looks promising, and the processing methods for it are being developed [2].

In this paper, the development and testing of a new method are presented. This method will use reflections of the collision alert radar to determine the state of the aircraft: its height and velocity with respect to the landscape. The method makes use of the wide aperture of the radar, as well as the signal filtering properties. It combines several surface reflections in front of the aircraft into one final aircraft state, and it can therefore provide ground collision warnings based on the landscape in front of the aircraft. This is not possible with existing equipment. This system has the potential to act as a terrain collision warning system for the pilot.

The underlying hardware and software principles of the state determination method are presented in Sec. III. This method is first tested in simulation experiments described in Sec. IV. The radar and the algorithm are subjected to a flight test, which is presented in Sec. V. The results of the flight are presented in Sec. VI, and a discussion on these is found in Sec. VII. Conclusions on the algorithms are given in Sec. VIII.

II. Algorithm Theory

Modern microwave sensing hardware and software has improved greatly in the past years, partly empowered by the arrival of self-driving cars [10–12]. Because of this, new systems can be developed that complement the shortcomings of current flight instruments [2]. In this section, the theoretical method for detecting the state is introduced. The hardware and software for this are described in two parts.

Received 16 September 2020; revision received 11 January 2021; accepted for publication 12 January 2021; published online 16 February 2021. Copyright © 2021 by the American Institute of Aeronautics and Astronautics, Inc. All rights reserved. All requests for copying and permission to reprint should be submitted to CCC at www.copyright.com; employ the eISSN 2327-3097 to initiate your request. See also AIAA Rights and Permissions www.aiaa.org/randp.

*Ph.D. Student, Kluyverweg 1; j.b.maas@tudelft.nl.

[†]Ph.D. Student, Kluyverweg 1.

[‡]Full Professor, Kluyverweg 1.

[§]Automatic Dependent Surveillance Broadcast/Cockpit Display of Traffic Information.

Table 1 Technical specifications of the radar hardware

Parameter	Value
Carrier frequency	9.425 GHz
Wavelength	31.83 mm
Sampling frequency	10 MHz
Pulse repetition frequency	4921 Hz
Power emitted	40 dBm
Bandwidth	10 MHz

A. Hardware

Frequency-modulated continuous-wave (FMCW) radar systems measure range and Doppler velocity (noted as r and V_r) of objects within sensor range [13]. The weight, cost, and power consumption are low enough that they can be taken on board of a small aircraft. If this is done, they can be used to sense the aircraft surroundings [14,15].

A collision alert radar system is developed for use in GA. This system is expected to increase situation awareness of GA pilots. The system is developed to have a wide aperture, up to 60 deg horizontally and vertically. Other aircraft can be seen with these radars and ground reflections are observed as well. Technical specifications of the hardware used can be found in Table 1.

An FMCW radar system can measure both the distance to and the Doppler velocity of an object [10,13], after antialiasing is performed [16,17]. The Doppler velocity is the component of the relative velocity in the direction of the object. Direction of arrival estimation can help localize a source of reflection in three dimensions [18,19].

B. Software

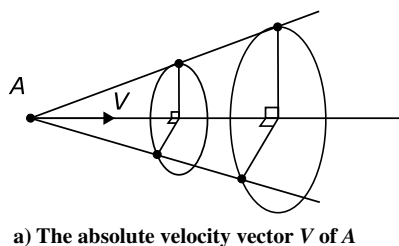
When the radar system is moving over a landscape, the surface can be represented by a collection of objects with different distances and relative radial velocities. The measured signals can be used to determine the instantaneous state of the system.

The landscape is modeled as an inertial flat plane that reflects emitted radar signals back to the system. The effect of this assumption will be investigated in Sec. III. Because the surface is not moving, the relative velocity vector is equal at all locations on the surface.

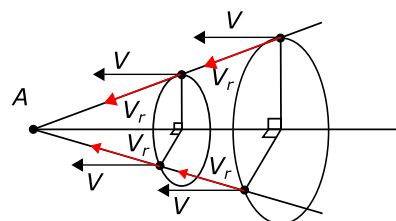
Radial velocity is defined as the component of the relative velocity vector in the direction of the object [17]. Because the relative velocity is the same everywhere, this is only dependent on the angle between the distance and velocity vectors of a point.

This means that two points will have an equal radial velocity only if the angles between the line from the aircraft to the point and the aircraft velocity vector are equal to each other. As illustrated in Fig. 1, this means that all points with the same radial velocity must lie on a three-dimensional cone around the system velocity vector.

A contour plot on the surface is created, connecting the points on the surface with equal radial velocity. Because all such points must lay on the three-dimensional cone and on the surface plane, the resulting curves are hyperbolas, parabolas, and ellipses. The transverse axes of the hyperbolas are the projection of the axis of the cones, i.e., the aircraft velocity vector. A second contour plot is added to the figure, connecting surface elements with the same distance to the system. The result is seen in Fig. 2.



a) The absolute velocity vector V of A



b) The relative velocity vectors of the points and their doppler velocities V_r

Fig. 1 Aircraft A and four points with the same angle between distance and velocity vector V forming a cone.

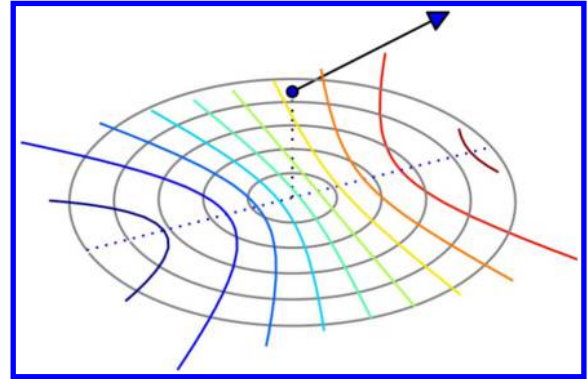


Fig. 2 Three-dimensional view of a system with a velocity above a flat surface, with contour plots of equal distance (gray) and radial velocity (colors).

From Fig. 2 it is observed that for a given distance to the system, multiple radial velocities exist. For this given distance, the maximal and minimal radial velocities can be found where the hyperbolas are tangent to the circle. Because the center of this circle lies on the transverse axes of the hyperbolas, the two types of contour plots must be tangent at the vertices of the hyperbolas, which is indicated as the dotted line in the figure.

This means that for a given distance to the system, the maximal and minimal radial velocities can be found at the transverse axis of the hyperbolas. This axis is the projection of the system velocity vector on the plane, which will be called the track vector. The track vector is illustrated in Fig. 3.

The FMCW radar can measure the distance and radial velocity of all points that form the surface. The following is now found: For a given distance, the surface points with the maximal and minimal radial velocities must lay on the track vector of the radar system. These points are significant, because they can be used to derive the aircraft state, as will be discussed in Secs. II.B.1 and II.B.2.

This is also given in mathematical notation. Say S is the collection of points p on the surface, and V is the velocity vector of the aircraft. Note $V_r(p)$ and $r(p)$ as the Doppler velocity and the range of p . Then it follows that

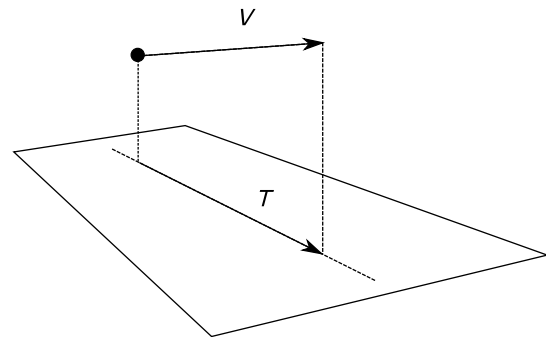


Fig. 3 Three-dimensional view of the track vector T as the projection of the velocity vector V on the ground.

$$S = \{p: p \text{ on surface}\} \quad (1)$$

$$S_x = \{p: p \in S, r(p) = x\} \quad (2)$$

$$T = \{p: p \in S, p \text{ below } V\} \quad (3)$$

$$p \in T \Leftrightarrow V_r(p) = \max\{V_r(s): s \in S_{r(p)}\} \quad (4)$$

1. State Finding Theory

In Fig. 4 a side view is given of a radar system above a surface. According to the theorem in the previous section, let point p be the point with the highest radial velocity V_R of all measurements with distance r . Therefore, point p must lay on the track vector of the radar system.

The radar system moves with a velocity of V_S . This means that the relative velocity vector of p is given as

$$V_p = -V_S = \begin{bmatrix} -V_X \\ -V_Z \end{bmatrix} \quad (5)$$

The radial velocity (which is measured) is a component of this relative velocity vector:

$$V_r = \frac{V_p \cdot r}{r} = \begin{bmatrix} -V_X \\ -V_Z \end{bmatrix} \cdot \begin{bmatrix} \sqrt{r^2 - H^2} \\ H \end{bmatrix} \frac{1}{r} \quad (6)$$

To get rid of the vector notation in Eq. (6), it is written out completely. Then calculus is applied to sort out the terms in groups of radar parameters r and V_r (which are measured) and system parameters V_X , V_Z , and H (which are unknown). These steps are as follows:

$$V_r \cdot r + V_Z \cdot h = -V_X \sqrt{r^2 - H^2} \quad (7)$$

$$(V_r \cdot r)^2 + 2V_r r V_Z H + (V_Z \cdot H)^2 = V_X^2 (r^2 - H^2) \quad (8)$$

$$(V_r \cdot r)^2 + 2V_r r V_Z H + H^2 (V_X^2 + V_Z^2) = r^2 V_X^2 \quad (9)$$

$$\frac{1}{V_X^2} (V_r \cdot r)^2 + \frac{2V_Z H}{V_X^2} V_r r + \frac{H^2}{V_X^2} (V_X^2 + V_Z^2) = r^2 \quad (10)$$

With multiple measurements of V_r and r , a set of equations can be constructed:

$$\begin{bmatrix} (V_{r_0} r_0)^2 & 2V_{r_0} r_0 H & H^2 (V_X^2 + V_Z^2) \\ (V_{r_1} r_1)^2 & 2V_{r_1} r_1 H & H^2 (V_X^2 + V_Z^2) \\ \vdots & \vdots & \vdots \\ (V_{r_n} r_n)^2 & 2V_{r_n} r_n H & H^2 (V_X^2 + V_Z^2) \end{bmatrix} \begin{bmatrix} a \\ b \\ c \end{bmatrix} = \begin{bmatrix} r_0^2 \\ r_1^2 \\ \vdots \\ r_n^2 \end{bmatrix} \quad (11)$$

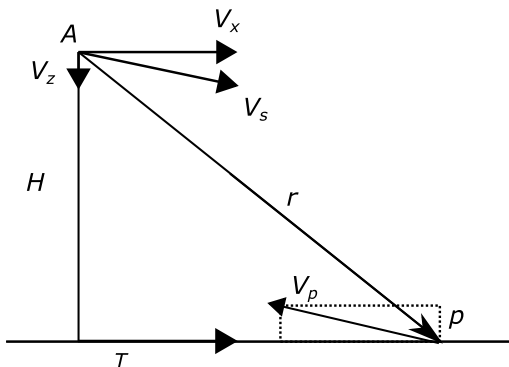


Fig. 4 Side view of the geometry between a moving aircraft A and a point p on the track vector T .

with the parameters

$$a = \frac{1}{V_X^2}$$

$$b = \frac{2V_Z H}{V_X^2}$$

$$c = \frac{H^2}{V_X^2} (V_X^2 + V_Z^2)$$

The equation is now in the form $AX = B$, with matrices A and B only containing measured data: V_r and r . The other three terms, a , b , and c , consist of combinations of V_X , V_Z , and H . These are unknown parameters, and they describe the state of the radar system: the velocities tangential and perpendicular to the landscape, and the height above it.

1. State Finding Method

If the radar can observe at least three surface points, a least squares solution to Eq. (11) can be found and parameters a , b , and c are known. Observing more points p increases the accuracy of the a , b , and c estimates. The aircraft state can then be computed as follows:

$$V_X = \sqrt{\frac{1}{a}} \quad (12)$$

$$V_Z = \frac{b}{\sqrt{4a^2 c - ab^2}} \quad (13)$$

$$H = \sqrt{c - \frac{b^2}{4a}} \quad (14)$$

The challenge is to observe multiple suited surface points with values of V_r and r . The reflections that lay on the track vector must therefore be distinguished from the rest. This can be done in several ways, for example, with direction of arrival estimation [18]. In this paper, Eq. (4) is used, as introduced previously.

Using this theorem means that if all observed reflections are sorted in range bins [20], the track vector can be found by selecting the observation with the highest value for V_r . This will provide a set of data points with different values of r and V_r , with which it is possible to compute the aircraft state.

III. Verification by Simulation

A simulation experiment is performed to verify the performance of the state determination algorithm. This section is divided into two sections, which discuss the setup of the experiment and the simulated results.

A. Simulation Experiment Setup

As an experiment, a virtual flight is performed in the X-plane flight simulator. The flight was recorded, and the radar terrain reflections are simulated once per second. The chosen location is important, because the algorithm makes use of radar reflections of the local landscape. Therefore multiple flight locations are used for this experiment.

Because Eq. (4) is based on the assumption of a flat landscape, the locations are selected to violate this assumption in increasing order. Digital elevation maps (DEM) of Europe[†] are used to quantify the local variance in terrain height. The DEM is divided into pieces of about $1 \text{ km} \times 0.6 \text{ km}$, and of each segment the standard deviation (SD) of the landscape height is taken. In Fig. 5 the result is displayed as a heat map, where brighter regions have a more local variance in terrain height.

Five locations are selected for simulation testing. The first is the airfield of Deelen in the Netherlands, because this is the location where a flight test experiment is possible (as described in Sec. V). The other locations are coordinates in regions around Europe, which vary

[†]The DEMs are retrieved from <http://www.viewfinderpanoramas.org/>.

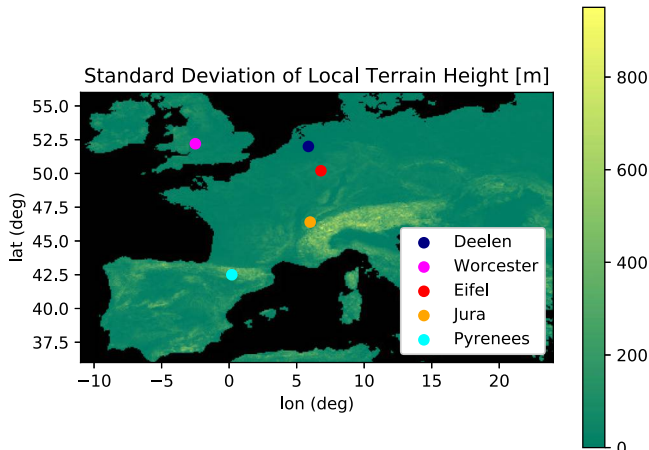


Fig. 5 Locations of the five simulation experiments within Europe.

from hilly to mountainous. These locations are in the west of England (near Worcester), the Eifel area, the Jura, and the Pyrenees. The coordinates are indicated on the map in Fig. 5. Also, a sixth simulation experiment is performed above a flat plane.

The same simulated flight is used for all experiments. The flight track is plotted over the elevation maps, as can be seen in Fig. 6. As can be seen, some flight locations are higher above mean sea level than others. The altitude of each flight is adjusted, in order to make sure that the average height above the landscape is the same for all simulations.

To check how the chosen test locations are related to the rest of the continent, a histogram is made in which the standard deviation of the local terrain elevation is counted for all DEMs available. This histogram (plotted on a logarithmic scale) is seen in Fig. 7. The values of the locations chosen are indicated in the figure as well. The values of Fig. 7 are also displayed in Table 2. The standard deviation of the local terrain elevation is given, as well as the percentage of the map in Fig. 5, which has a lower local SD than the location.

B. Simulation Experiment Results

The results for the height estimates are seen in Figs. 8 and 9. At first glance it is seen that the algorithm can approximate the simulated values for some of the simulations. For other flights, the results differ from the simulated truth.

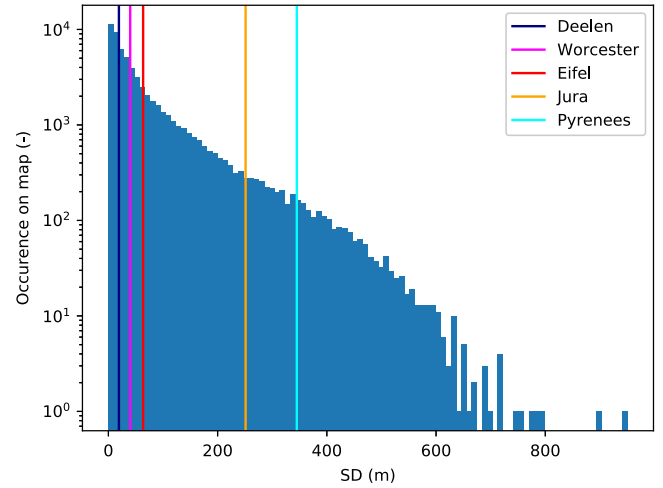


Fig. 7 Histogram of occurrences of local terrain SDs in the DEMs of Europe.

Table 2 Values of local terrain height SD and how this compares to the rest of Europe

Location	SD of local height, m	Part of Europe flatter, %
Flat terrain	0	0
Deelen	19.2	33.4
Worcester	39.9	52.68
Eifel	63.6	65.32
Jura	251.2	93.72
Pyrenees	345.0	97.24

As expected, the results deteriorate when the landscape has more height differences. The flat terrain simulations yield results that are very close to the simulated truth. Simulations above the Deelen area also provide consistent results, and this area was found to be hillier than 33.4% of Europe. For test areas such as the Jura and the Pyrenees the results are unreliable. These test locations represent about the most mountainous landscapes of Europe.

Numerical values of the height estimate differences can be seen in Table 3. The algorithm seems unsuitable for flight over mountainous

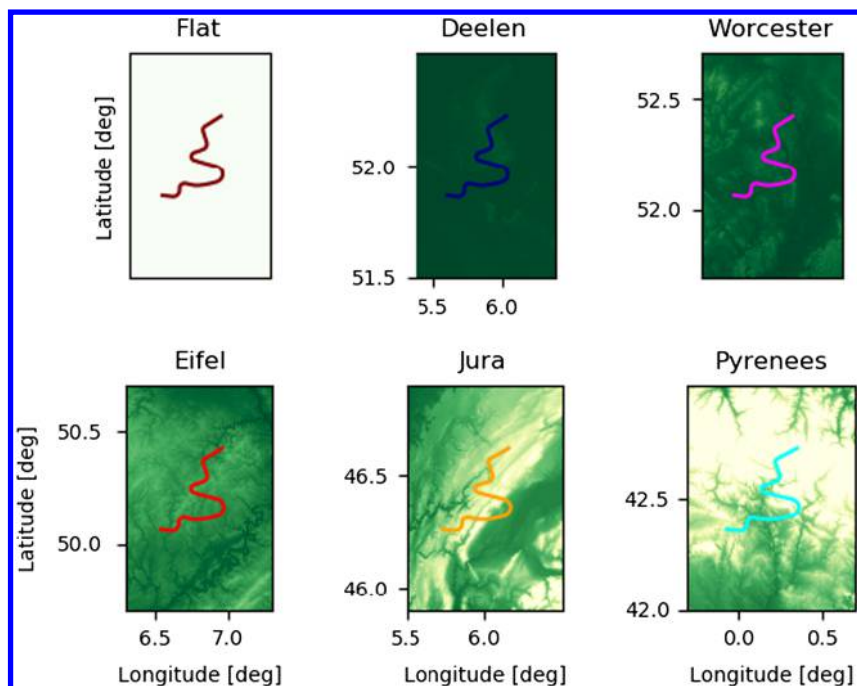


Fig. 6 Local DEMs at the simulation experiments' locations. Lighter colors indicate higher terrain. The flight tracks are drawn with colored lines.

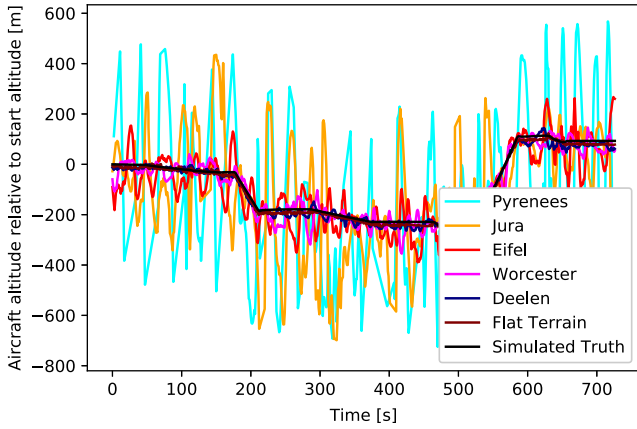


Fig. 8 Height results of the state algorithm for simulated radar data, and the true values.

regions, but it appears that the algorithm can provide accurate results when used above regions with low local height SD. It is also observed that a low-pass filter may help remove high-frequency noise from the results.

IV. Flight Experiment

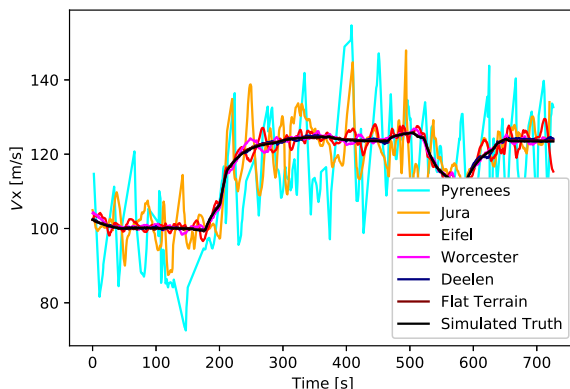
In Sec. III, the state finding method has been developed. Preliminary results from a simulation experiment indicate that the method can yield desired results. After this, the algorithms were used in a flight test in the Netherlands. This experiment is described in this section.

The aircraft used is a Pipistrel Virus, and two freight containers are attached to the wings. In the front of one of the containers is the radar hardware. The radar antennas have a range of 3 km and they are aimed to the front and downward, such that they can always receive reflections from the track vector. The radar measurements are able to determine the range to a reflection accurate within 20 m, and the radial velocity is accurate to 0.3 m/s. An image of the aircraft can be seen in Fig. 10, and the aperture and aim of the antenna are illustrated in Fig. 11.

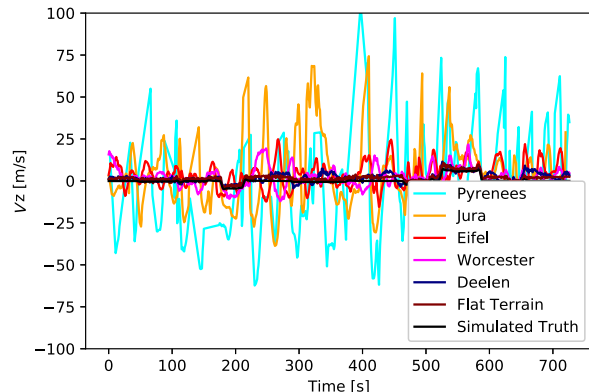
The flight was performed on October 23, 2019, under visual meteorological conditions. The location was the military airfield of Deelen, in the Netherlands, and the airspace was closed for other traffic. The pilot flew circuits around the airfield with increasing altitudes. The aircraft’s true location and velocity were measured using an on-board GPS device and they are plotted in Fig. 12. The FMCW radar was operational during the entire flight, including taxiing, similar to the GPS. The radar state results are compared with those of the GPS.

V. Results

The results of the experiment can be seen in Figs. 13 and 14. Both of these figures contain two subfigures. In Fig. 13 the velocity results are given in horizontal and vertical direction. In Fig. 14a the GPS results are seen unmodified. In Fig. 14b the GPS results have been



a) Horizontal velocity results



b) Vertical velocity results

Fig. 9 Velocity results of the state algorithm for simulated radar data, and the true values.

Table 3 Mean and standard deviation of height estimate errors of simulated flights at different locations

Location	Mean error, m	SD of the error, m
Flat terrain	8.5	6.5
Deelen	10.3	13.1
Worcester	11.3	35.8
Eifel	20.4	70.5
Jura	130.0	451.1
Pyrenees	381.7	821.6



Fig. 10 The test aircraft, with the radar in the port freight container.

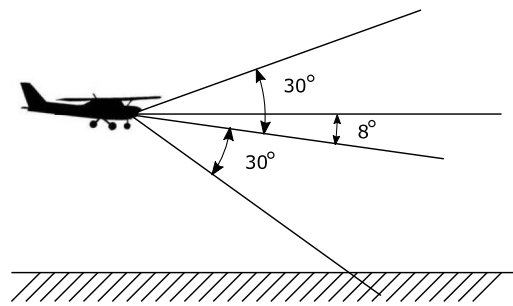


Fig. 11 The aperture and direction of the radar, as mounted on the aircraft.

calibrated such that the height above the published airfield altitude is given.

The light green line in the background is the raw radar data, and it can be seen that high-frequency variations are present. The first step in the computations is to apply outlier filtering and to discard data points of which the height differs by more than 150 m from the GPS data; 15% of the data were removed in this manner.

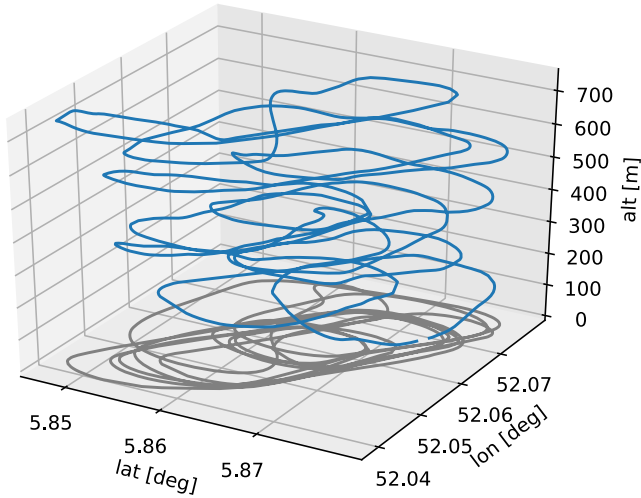


Fig. 12 The three-dimensional flight path, containing circuits of increasing altitude.

The other data results are fed to a simple Kalman filter to remove the variations of the signal [21]. Because the height and vertical speed are related to each other, the linear model for the filter used is

$$x := F \cdot x = \begin{bmatrix} 1 & 0 & 0 \\ 0 & 1 & 0 \\ 0 & -dt & 1 \end{bmatrix} \begin{bmatrix} V_x \\ V_z \\ h \end{bmatrix} \quad (15)$$

The negative sign in the equation is a consequence of V_z being defined positive downward, which is the opposite direction of H , as was seen in Fig. 3.

Similarly, it should be noted that the values for V_z in the Fig. 13b are also positive downward. Kalman filtering does improve the accuracy of the results, as expected. Numerical values of the results are displayed in Table 4.

From Table 4 it is seen that the estimates of the velocity have a small offset of several centimeters per second. The standard deviation is larger, in the order of several meters per second.

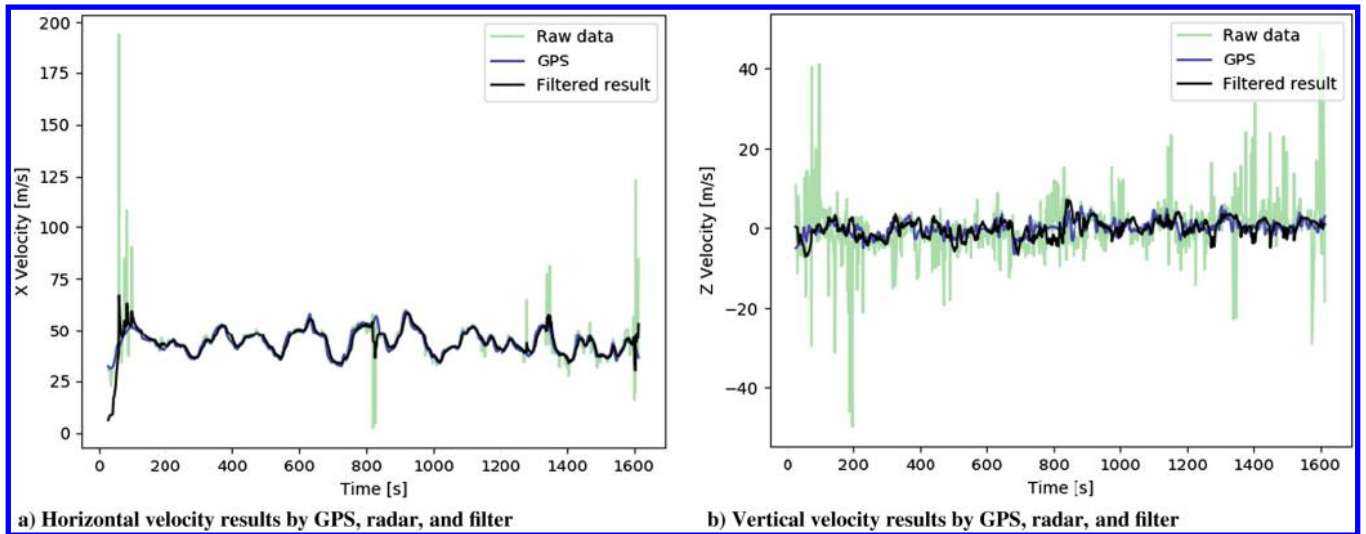


Fig. 13 Velocity results by GPS, radar, and filter.

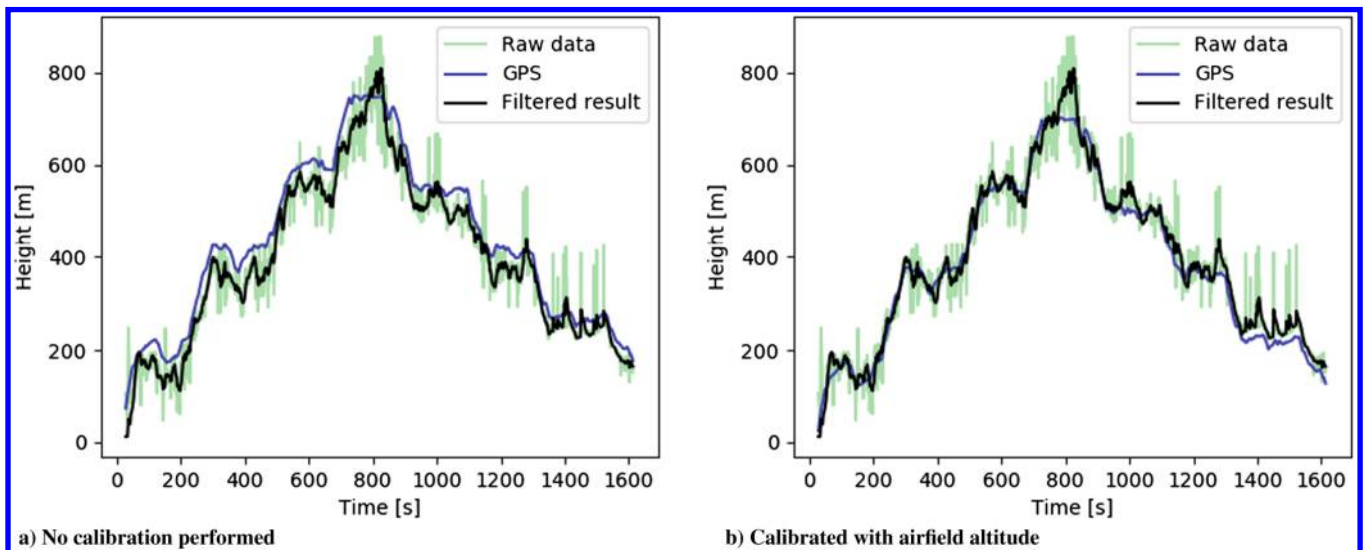


Fig. 14 Height results by GPS, radar, and filter.

Table 4 Results of the State Determination algorithm compared with a GPS recorder

Parameter	Raw data		Filtered results	
	Mean difference	SD	Mean difference	SD
V_X , m/s	-0.42	6.36	-0.19	2.99
V_Z , m/s	0.21	5.76	-0.13	1.98
H , m	36.27	36.83	36.57	23.82

It is also seen that the height measurements are on average 36 m off, and that their standard deviation is of equal size. This will be discussed in more detail in Sec. VII.

The Kalman filter removes high-frequency noise from the measurements and improves the results. The mean error of the velocity measurements becomes smaller, and the standard deviation is reduced for all measurements. Only the average difference in the altitude measurements does not improve when a Kalman filter is applied, but it is still around 36 m. This will be discussed further in the next section.

VI. Discussion

As noted in the previous section, the height difference between GPS and radar is on average 36 m off. The origin of this is the difference in GPS altitude and terrain elevation. Whereas GPS computes the altitude above the Earth model, the radar uses the reflections of the actual terrain. At the start of the flight, before takeoff, the GPS indicated an altitude of 35.97 m. This explains why the radar has a mean difference of about 36 m, or about 120 ft.

A solution to this GPS error can be to calibrate the height at the start of the flight, which will yield results similar to those in Fig. 14b. However, this solution guarantees only a local fix, and it does not prevent other faults in the landscape model either, including the height of trees. If relying only on GPS during a flight, a risk of terrain collisions is still present.

The height estimates are dependent on the position of the radar reflections. If trees are present, the radar signals will not reach the ground but reflect back on the leaves of the trees. A canopy of trees acts as a radar reflecting plane, parallel to the ground. This means that trees and other foliage increase surface height, and therefore decrease the radar height further. This is useful for the pilot, who wants to avoid flying into the canopy.

In Fig. 13a it is seen that the V_X measurements are often very close to the actual speed, but that they are several times distorted by a few outliers that have not been removed by the first filter. These outliers affect the mean error and standard deviation, and their influence is reduced effectively by a high-frequency noise filter. In this study a Kalman filter was used.

Apart from the height difference, it is observed that the algorithm accuracy is similar to the performance of the hardware, of which the range accuracy is within 20 m and the radial velocity accuracy is 0.3 m/s.

The vertical speed has more accurate results than the horizontal speed, which is surprising because the radar was pointed to the front of the aircraft. This meant that most of the reflections observed will lay in front of the aircraft, and therefore have a high horizontal radial velocity. It was therefore expected that the algorithm would be able to tell the horizontal velocity more accurately than the vertical velocity. The Kalman filter uses the relation between vertical speed and height, so extra information is available for a good estimate for both parameters. This can be a reason why the vertical velocity is more accurate.

Considering the uncertainties of the systems, it is found that the radar is less accurate than the GPS, but it is not dependent on a database to find the clearance to the ground. GPS determines the position relative to the Earth ellipsoid approximation with a horizontal accuracy of 4 m and a vertical accuracy of 8 m. For GPS altimetry, the uncertainty can be expressed as 8 m + ground database uncertainty + unknown height of trees. For the radar system, the standard deviation is 24 m.

Relating back to the theoretical model and the simulation experiment in Sec. IV, it is found that the state finding method is more accurate over flatter landscapes. As found from the digital elevation

maps, about 33.4% of the European land is flatter than the landscape around Deelen, which is the test area. This implies that state estimation is possible with this system above at least one-third of European land. For mountainous areas, however, it is unlikely that the method from this paper alone is sufficient. Future research may indicate in more detail at what locations this system can provide reliable results.

It should be noted that much space for improvement exists in the radar system. Better outlier filtering can have a significant impact on the V_X estimates, as well as the height tracking. Increasing the measurement rate can be of great influence on the Kalman filter results as well. This experiment was performed with one observation per second, but sampling rates of 10, 20, or 100 measurements per second are possible with modern-day radar systems.

As mentioned in the Introduction, the availability and performance of modern microwave sensors and processors have increased significantly over the past years. In the last five years, the price of the equipment used in this experiment has decreased by a factor of 40, and the gain of available antennas has increased by over 10 dB. It is possible that the accuracy of the raw results of the radar system will surpass that of the GPS system in the next decade, for a similar price. A pilot will then be able to use a radar system to provide ground collision warnings.

VII. Conclusions

In this paper a novel strategy for altitude and velocity determination was presented. The method is based on an on-board radar system and its reflections on the ground. It is therefore suitable for operations in the lower segments of the airspace, typically at altitudes used for GA.

The system was tested in a local flight. It is concluded that the velocity estimates of the radar can approach the quality of those of GPS navigation, if proper filtering techniques are applied.

It is found that the GPS can provide a more accurate altitude above a reference point than the radar. However, calibration was necessary for the GPS results but not for the radar. Also, the radar does observe tree height and landscape shape, which may be absent or unreliable in the GPS database. Radar altimetry may be a better option than using GPS, depending on what the data are used for.

Simulations experiments indicate that the radar method is expected to work above at least 33.4% of the European landscape. Further research can indicate the performance limits for the rest of Europe.

The quality of available radar hardware has increased significantly in the past years, and prices have decreased. If these trends continue, using a radar system to find flight state information can become a solution for pilots that do not wish to be dependent on the correctness of any databases.

Acknowledgments

This project has received funding from the European Union's Horizon 2020 research and innovation program [grant agreement no. 674744]. The funding was transferred to the company Selfly B.V., which relayed it to authors J. Maas and R. Van Gent to do the research. The company Selfly B.V. did not have any additional role in the study design, data collection and analysis, decision to publish, or preparation of the manuscript. These tasks were performed by Delft University of Technology. The only role of Selfly B.V. in this study was to provide logistical support.

References

- [1] Maas, J., Gent, R. V., and Hoekstra, J., "A Portable Primary Radar for General Aviation," *PLoS ONE*, Vol. 15, No. 10, 2020, pp. 1–32. <https://doi.org/10.1371/journal.pone.0239892>
- [2] Maas, J., Gent, R. V., and Hoekstra, J., "Object Tracking in Images of an Airborne Wide Angle FMCW Radar," *ICRAT International Conference for Research in Air Transportation*, Barcelona, 2018, p. 8.
- [3] "Problems in Worldwide Standardization of the Units of Height Measurement," Tech. Rept. FAA-EM-78-2, U.S. Department of Transportation, Federal Aviation Administration, 1978.
- [4] Ochieng, W. Y., Sauer, K., Walsh, D., Brodin, G., Griffin, S., and Denney, M., "GPS Integrity and Potential Impact on Aviation Safety," *Journal of Navigation*, Vol. 56, No. 1, 2003, pp. 51–65. <https://doi.org/10.1017/S0373463302002096>

- [5] Kao, W.-W., "Integration of GPS and Dead-Reckoning Navigation Systems," *Vehicle Navigation and Information Systems Conference*, Vol. 2, Troy, MI, 1991, pp. 635–643.
<https://doi.org/10.1109/VNIS.1991.205808>
- [6] Zhao, L., Ochieng, W. Y., Quddus, M. a., and Noland, R. B., "An Extended Kalman Filter Algorithm for Integrating GPS and Low Cost Dead Reckoning System Data for Vehicle Performance and Emissions Monitoring," *Journal of Navigation*, Vol. 56, No. 2, 2003, pp. 257–275.
<https://doi.org/10.1017/S0373463303002212>
- [7] Nitti, D., Bovenga, F., Chiaradia, M., Greco, M., and Pinelli, G., "Feasibility of Using Synthetic Aperture Radar to Aid UAV Navigation," *Sensors*, Vol. 15, No. 8, 2015, pp. 18,334–18,359.
<https://doi.org/10.3390/s150818334>
- [8] Maas, J., Stefanovici, V., Gent, R. V., and Hoekstra, J., "Validation of GPS by Ground Scanning Radar," *ICRAT International Conference for Research in Air Transportation*, 2020, pp. 1–0.
- [9] Nyfors, E., "Industrial Microwave Sensors—A Review," *Subsurface Sensing Technologies and Applications*, Vol. 1, No. 1, 2000, pp. 23–43.
<https://doi.org/10.1023/A:1010118609079>
- [10] Lee, M. S., and Kim, Y. H., "Design and Performance of a 24-GHz Switch-Antenna Array FMCW Radar System for Automotive Applications," *IEEE Transactions on Vehicular Technology*, Vol. 59, No. 5, 2010, pp. 2290–2297.
<https://doi.org/10.1109/TVT.2010.2045665>
- [11] Folster, F., Rohling, H., and Lubbert, U., "An Automotive Radar Network Based on 77 GHz FMCW Sensors," *IEEE National Radar Conference—Proceedings*, Vol. 2005, Jan. 2005, pp. 871–876.
<https://doi.org/10.1109/RADAR.2005.1435950>
- [12] Chavez-Garcia, R. O., and Aycard, O., "Multiple Sensor Fusion and Classification for Moving Object Detection and Tracking," *IEEE Transactions on Intelligent Transportation Systems*, Vol. 17, No. 2, 2015, pp. 525–534.
<https://doi.org/10.1109/TITS.2015.2479925>
- [13] Stove, A. G., "Linear FMCW Radar Techniques," *IEE Proceedings F Radar and Signal Processing*, Vol. 139, No. 5, Oct. 1992, pp. 343–350.
<https://doi.org/10.1049/ip-f-2.1993.0019>
- [14] Naulais, C., "General Aviation Radar System for Navigation and Attitude Determination," MSc. Thesis, Technische Universiteit Delft, Delft, The Netherland, 2015.
- [15] Meta, A., *Signal Processing of FMCW Synthetic Aperture Radar Data*, TU Delft, Delft, The Netherland, 2006.
- [16] Zhang, J., and Wang, S., "An Automated 2D Multipass Doppler Radar Velocity Dealiasing Scheme," *Journal of Atmospheric and Oceanic Technology*, Vol. 23, No. 9, 2006, pp. 1239–1248.
<https://doi.org/10.1175/JTECH1910.1>
- [17] Orfanidis, S. J., *Introduction to Signal Processing*, Vol. 1, Prentice Hall, Upper Saddle River, NJ, 1972.
<https://doi.org/10.1109/TCOM.1972.1091274>
- [18] Weiss, A. J., and Friedlander, B., "Eigenstructure Methods for Direction Finding with Sensor Gain and Phase Uncertainties," *Circuits, Systems, and Signal Processing*, Vol. 9, No. 3, 1990, pp. 271–300.
<https://doi.org/10.1007/BF01201215>
- [19] Shaw, A. K., "Improved Wideband DOA Estimation Using Modified TOPS (mTOPS) Algorithm," *IEEE Signal Processing Letters*, Vol. 23, No. 12, 2016, pp. 1697–1701.
<https://doi.org/10.1109/LSP.2016.2614310>
- [20] Koks, D., "How to Create and Manipulate Radar Range-Doppler Plots," Defence Science and Technology Organisation Tech. Rept. DSTO-TN-1386, Edinburgh, 2014.
- [21] Welch, G., and Bishop, G., *An Introduction to the Kalman Filter*, Vol. 8, Univ. of North Carolina, Chapel Hill, NC, 2001, pp. 1–81.
<https://doi.org/10.1.1.117.6808>

P. Wei
 Associate Editor